# Iris Recognition in Visible Wavelengths and Unconstrained Conditions

Hugo Proença

**Abstract** One of the most challenging goals in biometrics research is the development of recognition systems to work in unconstrained environments and without assuming the subjects' willingness to be recognised. This has led to the concept of *non-cooperative recognition*, which broaden the application of biometrics to forensics / criminal seek domains. In this scope, one active research topic seeks to use as main trait the ocular region acquired at visible wavelengths, from moving targets and large distances. Under these conditions, performing reliable recognition is extremely difficult, because such *real-world* data have features that are notoriously different from those obtained in the classical constrained setups of currently deployed recognition systems. This chapter discusses the feasibility of iris / ocular biometric recognition: it starts by comparing the main properties of near-infrared and visible wavelength ocular data, and stresses the main difficulties behind the accurate segmentation of all components in the eye vicinity. Next, it summarises the most relevant research conducted in the scope of visible wavelength iris recognition and relates it to the concept of *periocular* recognition, which is an attempt to augment classes separability by using - apart from the iris - information from the surroundings of the eye. Finally, the current challenges in this topic and some directions for further research are discussed.

## 1 Introduction

The iris is one of the most valuable traits for human identification and growing efforts have been concentrated in the development of this technology [7]. Fundamentally, three reasons justify this interest: (1) it is a naturally protected internal organ that is visible from the exterior; (2) it has a near circular and planar shape that

Hugo Proença
IT: Instituto de Telecomunicações, University of Beira Interior, Covilhã, Portugal e-mail: hugomcp@di.ubi.pt

turns easier its segmentation and parameterization and (3) its texture has a predominantly phenotypic or chaotic appearance that is stable over lifetime. The accuracy of the deployed iris recognition systems is remarkable: a study of 200 billion cross-comparisons conducted by Daugman [15] reported false acceptance rates of order $10^{-6}$ with false rejections of 1%. Other independent evaluations ([30] and [47]) confirmed these results.

Current systems require high illumination levels, sufficient to maximize the signal-to-noise ratio in the sensor and to capture images of the discriminating iris features with sufficient contrast. However, if similar processes were used to acquire iris images from large distances, acceptable depth-of-field values would demand significantly higher f-numbers for the optical system, corresponding directly (squared) with the amount of light required for the process. Similarly, the motion factor will demand very short exposure times, which again will require too high levels of light. The American and European standards councils ([2] and [10]) proposed safe irradiance limits for near-infrared (NIR) illumination of near 10 mW / $cm^2$. In addition to other factors that determine imaging system safety (blue light, non-reciprocity and wavelength dependence), these limits should be taken into account, as excessively strong illumination can cause permanent eye damage. The NIR wavelength is particularly hazardous, because the eye does not instinctively respond with its natural mechanisms (aversion, blinking and pupil contraction).

The pigmentation of the human iris consists mainly of two molecules: brown-black Eumelanin (over 90%) and yellow-reddish Pheomelanin [48]. Eumelanin has most of its radiative fluorescence under the visible wavelength (VW), which—if properly imaged—enables the capture of a much higher level of detail, but also of many more artefacts, including specular and diffuse reflections and shadows. Also, the spectral reflectance of the sclera is significantly higher in the VW than in the NIR and the spectral radiance of the iris in respect of the levels of its pigmentation varies much more significantly in the VW than in the NIR. These optical properties are the biological roots behind the higher heterogeneity of the VW iris images, when compared with the traditional NIR data. Also, the types and number of artefacts likely to appear in VW and NIR data are notoriously different, which justify the need for specialized recognition strategies.

Fig. 1 illustrates the variations in appearance of NIR and VW images, with respect to the levels of iris pigmentation. These images were acquired using a multispectral device, in a synchronous way. It is particularly interesting to observe the inverse relation between the levels of minutia captured in NIR and VW data, with respect to the levels of iris pigmentation: while for light pigmented irises, much more detail is perceived in VW than in NIR images, it occurs the opposite for heavily pigmented irises (leftmost image). Note that this is a particularly concerning problem, as the large majority of the world population has heavily pigmented irises.

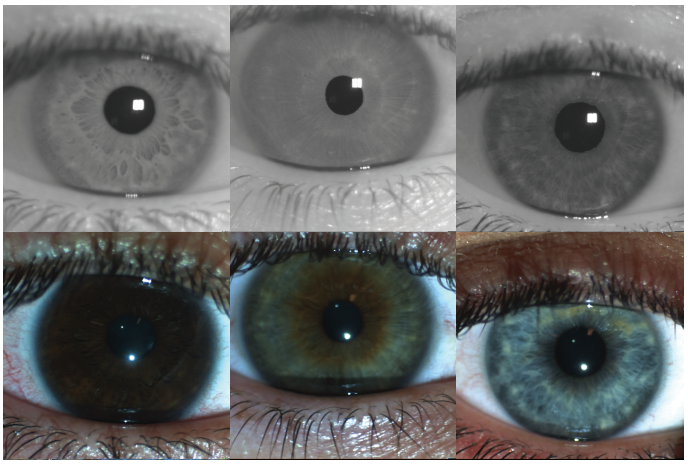


**Fig. 1** Comparison between the appearance of the iris texture acquired in a synchronous way, using multispectral sensors. The upper row gives the iris data in near-infrared (NIR) wavelengths, while the bottom row gives the corresponding data in visible wavelengths (VW). Note the inverse relationship in the NIR and VW data regarding the levels of iris pigmentation and the captured iris minutia.

## 2 VW Iris Recognition: Summary of Research Works

Tan *et* al. [80] performed biometric recognition according to both iris and periocular data. Global color-based features and local ordinal measures were used to extract discriminating data from the iris region, later fused to periocular data extracted from texton representations. Finally, fusion is performed by the sum rule using the normalized scores generated for the different types of features. Wang *et al.* [85] used an adaptive boosting algorithm to build a strong iris classifier learned from a set of bi-dimensional Gabor-based set of features, each corresponding to a specific orientation and scale and operating locally. Later, given the fact that the pupillary boundary is especially difficult to segment in VW data, the authors trained two distinct classifiers: one for irises deemed to be accurately segmented and another for cases in which the pupillary boundary was not accurately segmented. Santos and Hoyle [71] fused a set of recognition techniques that can be divided in two main categories: wavelet-based textural analysis methods applied to the iris region, complemented by distribution-based (histogram of oriented gradients and local binary patterns) and scale invariant feature transforms that analyze the periocular region, which was recently suggested as an important addition for handling degraded samples, essentially because it is less vulnerable to problems resulting from deficient illumination or low-resolution acquisition. Shin *et al.* [73] started by classifying the left and right eyes by their eyelash distributions, which they used to reduce the search space. Further, they coupled two encoding and matching strategies based in color and tex-

tural analysis to obtain multiple distance scores fused by means of a weighted sum rule, which is claimed to improve the separation between *match* and *non-match* distributions. Li *et al.* [33] used a novel weighted co-occurrence phase histogram to represent local textural features. This method is claimed to model the distribution of both the phase angle of the image gradient and the spatial layout, which overcomes the major weakness of the traditional histogram. A matching strategy based on the Bhattacharyya distance measures the goodness of match between irises. Finally, the authors concluded that the performance is improved when a simple image registration scheme accounts for the image deformation. Marsico *et al.* [35] proposed the use of implicit equations to approximate both the pupillary and limbic iris boundaries and perform image normalization. Next, they exploited local feature extraction techniques such as linear binary patterns and discriminable textons to extract information from vertical and horizontal bands of the normalized image. Li and Ma [32] introduced an image registration method based on the Lucas-Kanade algorithm to account for iris pattern deformation. Operating on the filtered iris images, this method divides the images into small sub-images and solves the registration problem for each small sub-image. Later, a sequential forward selection method searches for the most distinctive filters from a family of Gabor filters, concluding that a very small number of selected features are able to obtain satisfactory performance. Finally, Szewczyk *et al.* [77] presented a semi-empirical approach based on a reverse bi-orthogonal dyadic wavelet transform, empirically selecting a compactly supported bi-orthogonal spline wavelet for which symmetry is possible with FIR filters and three vanishing moments. The authors concluded that such a method produces a short biometric signature (324 bits) that can be successfully used for recognition under such challenging conditions, improving its reliability.

Du *et* al. [19] aimed at robustness and used the SIFT transform and Gabor wavelets to extract iris features, which were used for local feature point description. Then two feature region maps were designed to locally and globally register the feature points, building a set of deformable iris sub-regions that takes into account the pupil dilation/contraction and deformations due to off-angle data acquisition.

## 3 Data Acquisition: Frameworks and Major Problems

The term *constraint* refers to one of the factors that currently deployed systems impose, in order to perform recognition with enough confidence: subjects distance, motion and gaze direction and lighting conditions of the environment. These constraints motivate growing research efforts and became the focus of many recent proposals, among which the ”Iris-on-the-move” project [46] should be highlighted: it is a major example of engineering an image acquisition system to make the recognition process less intrusive for subjects. The goal is to acquire NIR close-up iris images as a subject walks at normal speed through an access control point. *Honeywell Technologies* applied for a patent [28] on a very similar system, which was also able to recognize irises at a distance. Previously, Fancourt *et* al. [20] concluded that

it is possible to acquire sufficiently high-quality images at a distance of up to ten meters. Narayanswamy and Silveira [51] used a wavefront coded optic to deliberately blur images in such a way that they do not change over a large depth-of-field. Removing the blur with digital image processing techniques makes the trade-off between signal-to-noise ratio and depth of field linear. Also, using wavefront coding technology, Smith *et* al. [75] examined the iris information that could be captured in the NIR and VW spectra, addressing the possibility of using these multispectral data to improve recognition performance. Park and Kim [54] acquired in-focus iris images quickly at a distance, and Boddeti and Kumar [6] suggested extending the depth-of-field of iris imaging frameworks by using correlation filters. He *et* al. [23] analyzed the role of different NIR wavelengths in determining error rates. More recently, Yoon *et* al. [90] presented an imaging framework that can acquire NIR iris images at-a-distance of up to three meters, based on a face detection module and on a light-stripe laser device used to point the camera at the proper scene region. Boyce *et* al. [8] studied the image acquisition wavelength of revealed components of the iris, and identified the important role of iris pigmentation. Although concluding that illumination inside the 700-900 nm optimally reveals the richness of the iris structure, they observed that irises with moderate levels of pigmentation could be imaged in the visible light with good quality.

### *3.1 Proof-of-Concept*

This section reports one possible solution for acquiring data of the ocular region from moving subjects in outdoor environments and large distances (between 10 and 40 meters), without requiring subjects' willingness to be recognised. A prototype was developed, with two cameras mounted on the exterior wall of the *SOCIA Lab.: Soft Computing and Image Analysis Lab.*[1], located in Covilhã, University of Beira Interior, Portugal. Cameras are at a first-floor level (approximately 5m above the ground), and pointing towards a parking lot. A master-slave configuration was adopted, i.e., a wide-view (static) camera (*Canon VB-H710F* in our prototype) covers the whole scene and provides data for human detection and tracking modules, which enables to point the PTZ camera (*Hikvision DS-2DE5286-AEL*) to subjects' faces. Fig. 2 illustrates the environmental conditions in this prototype and the data acquired by both the wide-view and PTZ devices.

In order to automatically obtain information from the subjects faces / ocular regions, the whole processing chain is composed by five modules: 1) at first, the SOBS [45] is used to discriminate between the background / foreground objects in the scene. Next, 2) a human detection algorithm based in the widely known Haar-based Viola and Jones algorithm [83] enables to obtain a set of regions-of-interest (ROI), which feed a 3) object tracking module, based in the KLT algorithm [72] and in the omega-shape of the head and shoulders region as primary source of keypoints.

[1] `http://socia-lab.di.ubi.pt`

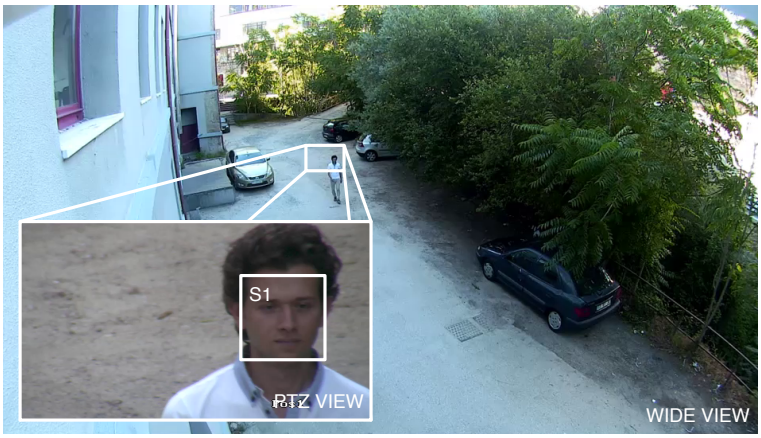


**Fig. 2** Image automatically captured using a master-slave configuration, that obtains high-resolution face images with inter-pupillary distance greater than 60 pixels, being subjects at 40 meters away from the cameras.

This tracker gives as output a set of point lists, each one describing the 2D position of one subject in the scene. Such positions are used by a 4) time-series predictor that estimates the subsequent positions of subjects in the scene, which is where the PTZ should be pointed to. A 5) camera calibration / synchronisation module is capable of accurately estimating the PTZ pan-tilt parameters without depending on additional constraints. Our approach exploits geometric cues to estimate subjects height and avoids depth ambiguity, obtaining the subject's 3D position in the scene. As main result of this processing chain, we get images similar to the ones illustrated in the bottom-left corner of Fig. 2.

In order to establish a baseline comparison between the performance attained by a face and a ocular recognizers, considering two classical algorithms: 1) the face recognition strategy proposed by Turk and Pentland [81], which introduced the concept of *eigenface* that became extremely popular in the computer vision literature; and 2) the periocular recognition algorithm due to Park *et* al. [55], defining a grid around the iris, from where histograms of oriented gradients, local binary patterns and scale-invariant features are extracted. Data from 25 persons were collected, with subjects from 15 to 30 meters away from the camera. In this case, only samples with relatively frontal pose (yaw $\pm\pi/10$) and *neutral* expression were kept, resulting in a total of 78,960 images pairwise comparisons. Fig. 3 compares the Receiver Operating Characteristic (ROC) curves obtained for the face and ocular recognition experts, being evident the better results of the ocular expert in the low *false acceptances* (FA) region, in contrast to the high FA region, where the facial recognition expert outperformed. In terms of the Area Under Curve (AUC) values, the ocular expert got 0.857, and the face expert 0.854, which are too close to provide statistically relevant conclusions about the *best* trait for this kind of environments. Note

that in this experiment all subjects had neutral facial expression, which otherwise would decay more the recognition performance of face than of the ocular region. Anyway, the main purpose of this experiment was exclusively to obtain a baseline performance that could be substantially improved by using more sophisticated recognition algorithms.

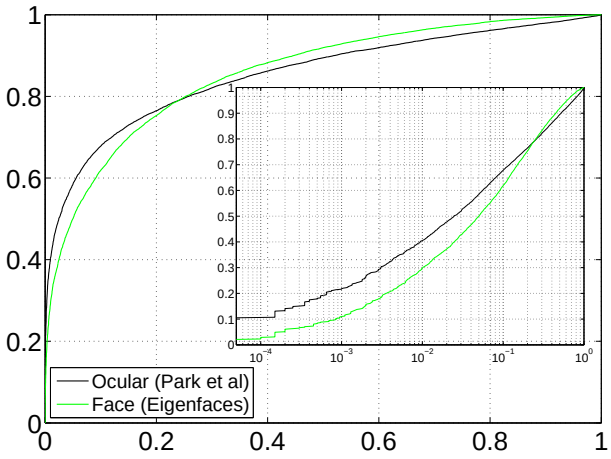


**Fig. 3** Comparison between the recognition performance observed for two classical face and ocular recognition algorithms, using data acquired in outdoor environments, under conditions that are currently associated to visual surveillance.

## *3.2 NIR vs. VW Data: Amount of Information Acquired*

As illustrated in Fig. 4, four freely available data sets were selected for all experiments reported in this chapter, each one representing a different data acquisition setup / scenario:

- The University of Bath data set[2] contains 32,000 NIR images from 800 subjects. From these, 6,000 images from 1.000 different classes (eyes) with very good quality were considered, to represent the optimal conditions for a recognition system. All irises are sharp, without relevant occlusions and in frontal view.
- The CASIA-Iris-Distance set[3] was collected by the CASIA long-range device in a relatively unconstrained setup. Images feature blink, motion blur, off-axis gaze

[2] http://www.smartsensors.co.uk/products/iris-database/32-000-full-set/

[3] http://biometrics.idealtest.org/

and other small anomalies, representing NIR data of moderate quality. A set of 9,521 images (127 subjects, 814 classes) was used, for which segmentation and noise detection was confirmed by visual inspection.

- The UBIRIS.v2 [60] dataset has 11,102 images from 261 subjects, acquired at visible wavelengths between three and eight meters away, under dynamic lighting conditions and unconstrained setups. Images are high heterogeneous in terms of quality, with glossy reflections across the iris, significant occlusions due to eyelids and eyelashes, off-angle and blurred data. 5,340 images from 518 classes were selected from this dataset, all of them accurately segmented. All these images were converted to grayscale.
- The FRGC [56] data set served initially for face recognition experiments and is a specially hard set for iris recognition, due to its limited resolution. The still images subset from both the controlled / uncontrolled setups was used. Images are typically frontal, with varying amounts of light, shadows and glossy reflections that occlude portions of the irises. 4,360 images from 868 classes were selected from this data set. All these images were reasonably segmented, according to visual inspection, and were converted to grayscale.

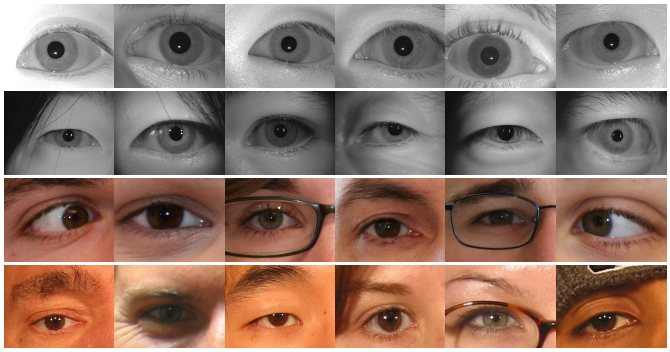

**Fig. 4** Examples of the data sets used in the experiments reported in this chapter. From top to bottom rows: BATH, CASIA-Iris-Distance, UBIRIS.v2, and FRGC datasets.

The first experiment comprised the comparison between the amount of information available in small iris patches, which was measured by the Shannon entropy criterion, quantifying (in terms of bits) the expected value for the amount of information in square regions $p \times p$ of the normalized image $\boldsymbol{I}$:

$$h(\boldsymbol{I}_{p\times p}) = -\sum_i P(\boldsymbol{I}_{p\times p} = i)\ \log_2\big(P(\boldsymbol{I}_{p\times p} = i)\big), \tag{1}$$

where $P(\boldsymbol{I}_{p\times p} = i)$ is the probability for the i$^{th}$ intensity in the patch.

Fig. 5 quantifies the amount of information in $p = 9$ patches. Even noting that the comparison between data sets might be unfair (the original images have different

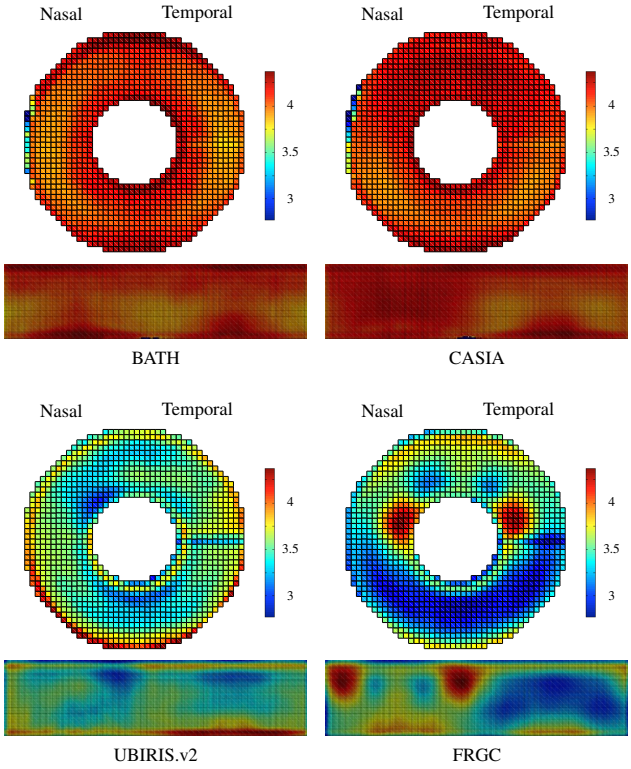


**Fig. 5** Average amount of information (Shannon entropy in $9 \times 9$ patches of the normalised images) across the different regions of the irises in the BATH, CASIA-Iris-Distance, UBIRIS.v2 and FRGC datasets. Values are expressed in bits, and enable to perceive the gap of information between NIR (BATH and CASIA) and VW (UBIRIS.v2 and FRGC) iris data.

resolution), the immediate conclusion is the higher homogeneity of values observed in NIR data than in the VW case. Note that the average values are also much higher in NIR than in VW data, which actually implies that the NIR images provide more heterogeneity in terms of intensities in iris patches than VW data.

Also, we observed that the pupillary regions are the most valuable in NIR images, which is not evident in VW. Regarding the FRGC dataset, there are two regions near the pupillary boundary with values notoriously higher than the remaining regions. We confirmed that they are due to frequent reflections not detected by the noise-free segmentation phase. Also, we noticed that in the FRGC set the bottom parts of the irises have evidently smaller amounts of information than the upper parts, probably due to the lighting sources from above that cause shadows in these regions.

# 4 Iris Segmentation

## *4.1 Comparison of NIR vs. VW Issues*

In order to acquire iris data from large distances and under unconstrained protocols, acceptable depth-of-field values demand high f-numbers for the optical system, corresponding directly (squared) with the amount of light required. Similarly, the motion factor demands very short exposure times, which again increases the amounts of light required. It is known that excessively strong illumination cause permanent eye damage and the NIR wavelength is particularly hazardous, because the eye does not instinctively respond with its natural mechanisms: aversion, blinking, and pupil contraction.

The above points were the major motivations for using visible-light to *in-the-wild* iris biometrics, even though such light spectrum increases the challenges in performing reliable recognition. As stated above, the pigmentation of the human iris enables to capture much higher level of detail in VW than in NIR, but also more noisy artefacts, including specular and diffuse reflections and shadows. In practice, this supports the uniqueness of the iris texture acquired in the visible-light spectrum (in a way similar to the empirically suggested for the near-infrared setup in previous studies [15]), but also stresses the difficulties in obtaining good quality data.

## *4.2 Why Is It So Difficult?*

There are four families of factors that affect the quality of VW iris biometric data not acquired under the classical *stop-and-stare* protocol: A) blur; B) occlusions; C) perspective and D) lighting. By working in a broad range of distances and on moving targets, blurred (A.1) and low-resolution (A.2) images are highly probable. Also, portions of the iris texture are occluded by eyelids (B.1), eyelashes (B.2) and glossy reflections (B.3) from the surrounding environment. Camera-to-subject misalignments may occur, due to subjects gaze (C.1) and pose (C.2). Finally, variations in light intensity (D.1), type (D.2) and incident angles (D.3) reinforce the broadly varying features of this kind of data.

Considering that periocular biometrics uses data not only from the iris but also from the surroundings of the eye (e.g., eyelids, eyebrows, eyelashes and skin), particular attention should be paid to additional data degradation factors, such as (E.1) makeup, (E.2) piercings and (E.3) occlusions (e.g., due to glasses or hair).

Fig. 6 illustrates the four families of factors that primarily affect the quality of data that is not acquired under the classical *stop-and-stare* protocol. By working in a broad range of distances and on moving targets, blurred (I.a) and low-resolution images (I.b) are highly probable. Also, portions of the iris texture are occluded by eyelids, eyelashes (II.c) and by glossy reflections from the surrounding environment (II.d). Camera-to-subject misalignments might occur, due to varying subjects gaze

(III.e) and pose (III.f). Finally, variations in light intensity, type and angle (IV. g and h) reinforce the broadly varying features of the resulting data.

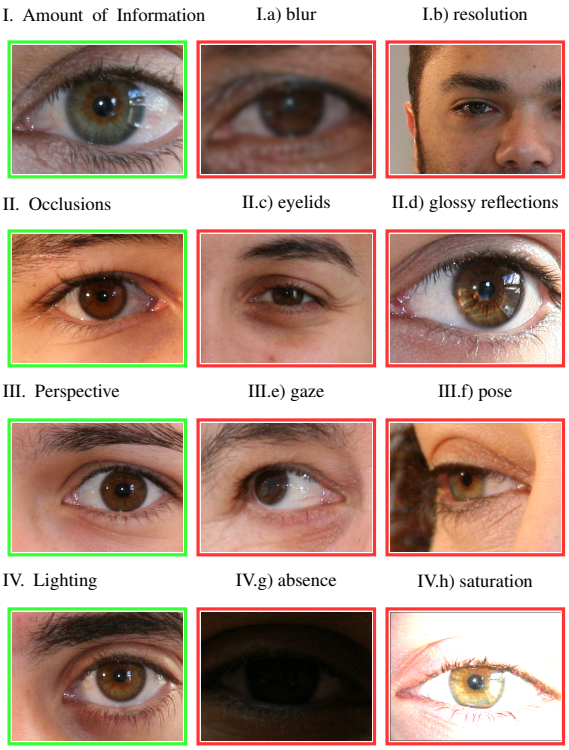


**Fig. 6** Four major types of variability in ocular data acquired in non-constrained setups. The amount of information highly varies, due to optical defocus, motion blur and data resolution (group I). Portions of the iris texture are often occluded by eyelids, eyelashes and reflections (group II) and subjects are misaligned with respect to cameras (group III). Finally, light sources of different type, intensity and 3D angles may exist in the environment (group IV).

## *4.3 Iris Segmentation: Summary of Research Works*

Segmentation is undoubtedly perhaps the most concerning phase of the processing chain, in terms of the ability of the whole system to deal with data that is degraded, due to the unconstrained acquisition setup. Also, as it is one of the earliest phases of the recognition process, it is the one that more directly has to deal with data variability and supports the whole process, with any error in segmentation (even small inaccuracies in one of the detected boundaries), easily propagating though the

processing chain and substantially increasing the recognition error rates [62]. Here we briefly summarise some of the most relevant research in the iris segmentation topic, not only covering methods for VW data, but also describing the approaches designed for NIR images, in order to stress the typical differences between both kinds of methods.

In Table 1 we give an overview of the main techniques behind several recently published iris segmentation methods. We compare the methods according to the data sets used in the experiments, categorized by the order in which they segment iris borders. The "Experiments" column contains the iris image databases used in the experiments. "Pre-processing" lists the image preprocessing techniques used before segmentation. Ord. Borders lists the order in which the iris borders are segmented, where $P$ denotes the pupillary borders and $S$ denotes the scleric iris borders ($x \rightarrow y$ denotes the segmentation of $y$ after $x$ and $x, y$ denotes independent segmentation, i.e., when no information from one parameterised border is used in the segmentation of the other). Pupillary Border and Scleric Border columns refer to the main methods used to segment that iris border.

Noting that the significant majority of the methods were designed to work with NIR images. These methods expect to find typically a high contrast between the pupil (almost black) and the iris, which justifies the order in which almost all of these NIR method segment both boundaries ($P \rightarrow S$). In contrast, methods that were particularly designed to handle VW data almost invariantly segment the outer iris boundary first, and then use this information to constrain the region where the pupillary boundary is searched, as there is almost no contrast between the pupil and the iris, in case of heavily pigmented irises, imaged with reduced amounts of light. Among the relevant innovations in this topic, techniques such as the use of active contour models, either geodesic ([70]), based on Fourier series ([16]) or based on the snakes model ([3]) can be highlighted. Noting that these techniques require previous detection of the iris to properly initialize contours, they are associated with heavy computational requirements. Modifications to known form fitting methods have also been proposed, essentially to handle off-angle images (e.g., [95] and [82]) and to improve performance (e.g., [44] and [18]). Finally, the detection of non-iris data that occludes portions of the iris ring has motivated the use of parabolic, elliptical and circular models (e.g., [4], and [18]) and the modal analysis of histograms [16]. Even so, in unconstrained conditions, several authors have suggested that the success of their methods is limited to cases of image orthogonality, to the non-existence of significant iris occlusions, or to the appearance of corneal reflections in specific image regions.

## 5 Image Quality Assessment

The concept of *good* metric is not trivial to determine, although the best one should maximally correlate with recognition effectiveness. Previous studies reported significant decays in effectiveness when data is degraded by each of the factors listed

**Table 1** Summary of the most relevant iris segmentation techniques.

| Method | Experiments | Preprocessing | Ord. Borders | Pupillary Border | Scleric Border |
|---|---|---|---|---|---|
| Zuo *et* al. [95] | CASIA.1, ICE, WVU (NIR) | Specular reflections detected (threshold), PDE and impainting | P → S | Randomized Elliptical Hough Transform | Weighted Integro-differential operator |
| Puhan *et* al. [66] | UBIRIS (VW) | Image binarization (threshold of the local Fourier spectral density) | S | - | Construction of a set of unidimensional signals, gradient analysis |
| Ross and Shah [70] | CASIA.1, WVU (NIR) | 2-D Median filter | P → S | Binarization (threshold), Circular Hough Transform | Geodesic Active Contours |
| Poursaberi and Araabi [57] | CASIA.1 (NIR) | Negative image, impainting | P | Iterative expansion/shrink of the detected border based on morphological operators | - |
| Morimoto *et* al. [49] | Non-specified (NIR) | Not described | P → S | Images difference | Images cascade at different scales, Sobel edges detection, elliptical form fitting |
| Liu *et* al. [44] | ICE (NIR) | Not described | P → S | Angular constrained Canny edge detection, Hough-based transform | Hough-based form fitting, hypothesis and test process |
| Kennell *et* al. [40] | BATH (NIR) | Histogram equalization, image binarization (threshold) | P → S | Morphological operators, integro-differential operator | Image binarization based on pixels+ neighborhood variance, form fitting |
| Vatsa *et* al. [82] | UBIRIS, CASIA.v3 (NIR, VW) | Not described | P → S | Rough estimation according to an elliptical model, followed by a modified Mumford-Shah functional | Process similar to the pupillary border |
| Proena and Alexandre [58] | UBIRIS (VW) | Histogram equalization | S → P | Feature extraction (pixel position + intensity) and fuzzy clustering to reduce image heterogeneity, Canny edges detection and circular Hough transform | Process similar to the pupillary border |
| Zaim [91] | CASIA.1 (NIR) | Morphologic operators to eliminate eyelashes | S → P | Split and merge process to localize regions of uniform intensity | Image normalization based on pupil coordinates, Sobel filtering, detection of horizontal edges in the normalized image |
| Broussard *et* al. [9] | BATH (NIR) | Not described | P,S | Extraction of local texture features, feed forward neural network | Process similar to the pupillary border |
| He and Shi [22] | Non-specified (NIR) | Image binarization, morphologic operations | P → S | Geometrical projection methods, Sobel filtering, form fitting | Canny edge extraction, Hough transform |
| Basit and Javed [4] | BATH (NIR) | Image binarization, morphologic operations | P → S | Iterative bijections-based method | Maximization of the difference of intensities of radial direction |
| Arvacheh and Tizhoosh [3] | CASIA.1 (NIR) | Not described | P → S | Near circular active contour model (snakes), interpolation process to improve performance | Integro-differential operator |
| Daugman [16] | ICE (NIR) | Not described | P → S | Active contours based on Fourier series, modeled with 17 discrete Fourier coefficients | Active contours based on Fourier series, modeled with 4 discrete Fourier coefficients |
| He *et* al. [24] | CASIA.1 (NIR) | Not described | P → S | Adaboost based object detection, iterative circumference shifting | Image normalization, Sobel and Canny filtering, line fitting |
| Zheng *et* al. [93] | SJTU (VW) | Conversion into Hsv color space | P → S | Assume existence of specular reflections, maximization of integral projections, integro-differential operator | Iterative shift, shrink and expand circumference process to minimize average intensity |
| Xu and Shi [87] | CAS-PEAL (VW) | Not described | P → S | Integral projection functions, median filtering, circumference shifting based on average intensity minimization | Sobel filtering, Edges weighting according to position and curvature |
| Honeywell International [29] | CASIA.1 (NIR) | Not described | P | Search for radial texture discontinuities | - |
| Dobes *et* al. [18] | AR, CVL (VW) | Histogram equalization, Gaussian blur | S | - | Canny edges detection, Angular constrained Hough transform |
| Shuckers *et* al. [74] | WVU (NIR) | Remove specular reflections (threshold), impainting | P → S | Elliptical integro-differential operator | Elliptical integro-differential operator |
| Tan *et* al. [78] | UBIRIS.v1, UBIRIS.v2 | Image clustering to perform rough eye localization | P, S | Integro-differential constellation | Integro-differential constellation |
| Proenca[61] | UBIRIS.v2, FERET, FRGC (VW), ICE 2006 (NIR) | Sclera Detection | $S \rightarrow P$ | Local hue, blue luminance, red chroma, neural network classification, constrained polynomial fitting | Local hue, blue luminance, red chroma, neural network classification, constrained polynomial fitting |

in Table 2. Here, we overview the main techniques used to assess iris image quality with respect to each factor and compare them according to the spectrum of light used, the type of analyzed data (*raw* image, *segmented* or *normalized* iris region) and their output (*local* or *global*), as they operate at the pixel or image level. We note that most of the methods operate on NIR images and assess quality in the segmented data (either in the cartesian or polar coordinate systems). Exceptions are usually related with focus measurement, obtained by one of two approaches: (1) measuring the high frequency power in the 2D Fourier spectrum through a high-pass convolution kernel or wavelet-based decomposition ([16], [31] and [11]); (2) analyzing

the sharpness of the iris borders through the magnitude of the first and second order derivatives ([1] and [92]). Another key characteristic is the level of analysis: some methods operate globally (at the image level), usually to determine focus, gaze or motion blur ([31], [38] and [84]). As image quality varies across the iris, others operate at the pixel level to determine local obstructions ([1], [36] and [59]). Motion is estimated by detecting interlaced raster shear that might be due to significant movements during the acquisition of a frame ([17], [34], [86] and [97]). Other approaches rely on the response of the convolution between the image and directional filters, being observed that linear motion blurred images have higher central peak responses than sharp ones ([36] and [39]). Gaze is estimated by 3D projection techniques that maximize the response of the Daugman's integro-differential operator [36] and by the length of the axes of a bounding ellipse [97]. Eyelids are detected by means of line and parabolic Hough transforms [25], active contours [41] and machine learning frameworks [59] [89]. The modal analysis of the intensities histogram enables the detection of eyelashes [16] [25], as do spectral analysis [34] and edge-based methods [36]. As they usually are the brightest regions of images, specular reflections are detected by thresholds [36], while diffuse reflections are exclusive of VW data and more difficult to discriminate, being reported a method based in texture descriptors and machine learning techniques [59]. Proença proposed a method [63] to assess the quality of VW iris samples captured in unconstrained conditions, according to the factors that are known to determine the quality of iris biometric data: focus, motion, angle, occlusions, area, pupillary dilation and levels of iris pigmentation. The key insight is to use the output of the segmentation phase in each assessment, which permits to handle severely degraded samples that are likely to result of such imaging setup.

## 6 Feature Encoding

Feature encoding is a particularly interesting sub-topic in the *unconstrained recognition* domain, due to the reduced quality of the data that is expected to be acquired. Here, a fundamental property of the iris texture should be considered, being one of the major reasons that justify the interest on this trait for this kind of scenarios: most of the discriminating information between the iris texture of different subjects lies in the lowest and middle-low frequency components, which are (luckily) those that are most easy to capture under outdoor environments and unconstrained acquisition protocols.

A particularly interesting advance is the use of Multi-Lobe Differential Filters, which are claimed to adapt better than the traditionally used Gabor filters to data of reduced quality and can be used at reduced computational cost. On the other way, they lie in a parameterisation space of much higher dimension than the one of Gabor filters, making more difficult to obtain good parameterisations for a specific recognition system / environment.

**Table 2** Overview of the most relevant methods published to assess the quality of iris biometric data.

| Method | Experiments Data Sets | Images | Analysis | Quality Assessment |
|---|---|---|---|---|
| Abhyankar and Schuckers[1] | CASIA.v3, BATH, WVU and Clarkson (NIR) | Segmented | Local, global | Occlusion (frequency analysis); focus (second order derivatives); contrast (hard threshold) and angular deformation (assigned manually) |
| Chen *et* al. [11] | CASIA.v3, WVU (NIR) | Segmented | Local, global | Focus and amount of information (2D isotropic Mexican hat wavelet-based frequency analysis) |
| Daugman and Downing[17] | ICE (NIR) | Raw data | Global | Effect of image compression; motion (interlaced raster shear) |
| Daugman [16] | ICE-1 (NIR) | Segmented | Local, global | Focus (magnitude of the response to a $5 \times 5$ high-pass kernel); off-angle (projective deformation that maximizes the circular shape of the pupil); eyelashes (intensities histogram modality) |
| Grabowski *et* al. [21] | - | Segmented and normalized | Global | Focus (entropy in the iris ring) |
| He *et* al. [25] | CASIA.v3 (NIR) | Segmented | Local | Eyelid (line Hough transform); eyelashes (intensities histogram modality) |
| Hollingsworth *et* al. [26] | Univ. Notre Dame (NIR) | Segmented | Global | Effect of pupil dilation |
| Jang *et* al. [31] | Yonsei (NIR, UBIRIS.v1 (VW) | Raw data | Global | Focus (ratio between the higher and lower frequency components, resultant of the dyadic discrete wavelet transform) |
| Kalka *et* al. [36] | CASIA.v3, WVU, ICE (NIR) | Segmented | Local, global | Focus (response to the Daugman's $8 \times 8$ high pass kernel); occlusion (morphologically dilated horizontal edges); motion blur (response to directional filters in Fourier space); off-angle (maximization of the circular integro-differential operator); specular reflection (threshold); lighting variation (intensities variance within small iris blocks); iris size (proportion of occluded pixels) |
| Kang and Park [37] | CASIA.v2(NIR) | Raw data | Global | Focus (magnitude of the response to a $5 \times 5$ high-pass kernel) |
| Kang and Park [38] | CASIA (NIR) | Segmented | Local | Eyelids (parabolic form fitting); focus (magnitude of the high frequency components; eyelashes (adaptive criteria according to the image blurring, convolution kernel for multiple eyelashes, first order differential for separable eyelashes) |
| Kang and Park [39] | CASIA.v3 (NIR) | Segmented | Local, global | Iris size; reflections (threshold); eyelids (parabolic form fitting scheme); eyelash (template matching based on continuity); motion blur (directional filters) and focus (frequency analysis) |
| Krishen *et* al. [41] | ICE (NIR) | Segmented and normalized | Local | Eyelids and eyelashes (gradient vector flow-based active contours method); focus (Gaussian mixture model learned from a set of image intensity histograms) |
| Nandakumar *et* al. [50] | WVU (NIR) | Segmented and normalized | Local, global | Focus and amount of information (2D isotropic Mexican hat wavelet-based frequency analysis) |
| Lu *et* al. [34] | CASIA.v3 (NIR) | Segmented and normalized | Local, global | Focus (energy of the frequency components resultant of a wavelet packet decomposition ); motion blur (average difference of intensities between adjacent rows); eyelids (hard threshold) and eyelashes (frequency analysis in the upper and lower iris extremes) |
| Proena and Alexandre. [59] | UBIRIS.v1 (VW) | Segmented and normalized | Local | Glossy and specular reflections, eyelids and eyelashes (extraction of an 8D feature set, neural network classification scheme) |
| Proença. [63] | UBIRIS.v2 (VW) | Segmented | Local, Global | Focus (response kernel), motion (directional derivative analysis), angle (analysis of bounding box), iris pigmemntation (HSV analysis) |
| Wan *et* al. [84] | SJTU-IDB (NIR) | Raw data | Global | Focus (magnitude of the response to a 2D isotropic Laplacian of Gaussian kernel) |
| Wei *et* al. [86] | CASIA.v2 (NIR), UBIRIS.v1 (VW) | Raw data and segmented | Global | Focus (magnitude of high frequency components); motion blur (average difference of intensities between adjacent rows) and occlusions (thresholds) |
| Ye *et* al. [89] | CASIA, CASIA.v2 (NIR) | Raw data | Global | Iris occlusions and focus (pixels intensity feed neural network that detects the iris contour. A second network gives the data quality). |
| Zhang and Salganicoff [92] | - | Segmented | Global | Focus (sharpness of a portion of the pupillary border, based in the gradients' magnitude) |
| Zuo and Schmid [96] | CASIA.v2, WVU (NIR) | Segmented | Global | Pupil size (threshold); pupillary and scleric borders sharpness (cumulative gradient along the boundaries) and ROI homogeneity (difference between average intensities of the iris, pupil and sclera) |
| Zuo and Schmid [97] | ICE, MBGC (NIR) | Segmented | Local, Global | Interlacing (average difference between odd and even rows); illumination (average intensity of the segmented iris); lighting (intensity variance over small iris blocks); occlusions (proportion of occluded iris pixels); area (pixel count); pupil dilation (proportion between the iris and pupil); off-angle (ratio between the major and minor axis of a bounding ellipse) and blur (magnitude of the high frequency components) |

## *6.1 Gabor vs. Multi-Lobe Differential Filters*

The discriminating power provided by each region of VW and NIR iris images was assessed, with respect to two families of filters: 1) Gabor kernels, which faithfully model simple cells in the visual cortex of mammalian brains [13] and are used in the most acknowledged iris recognition algorithm; and 2) Multi-lobe differential filters (MLDF), which were recently reported as a relevant advance in the iris recognition field [76].

The impulse response of a Gabor kernel is defined by the multiplication of a harmonic and a Gaussian function:

$$\boldsymbol{G}[x,y,\omega,\varphi,\sigma] = \exp\left[\frac{-x^2-y^2}{\sigma^2}\right]\exp[2\pi\omega i\Phi], \tag{2}$$

where $\Phi = x\cos(\varphi)+y\sin(\varphi)$, $\omega$ is the spatial frequency, $\varphi$ is the orientation and $\sigma$ the standard deviation of a Gaussian kernel (isotropic in our experiments, $\sigma = 0.65\omega$). A more general form of Gabor filters can be found in the literature (e.g., [15]), allowing for different scales along the axes ($\sigma_x$ and $\sigma_y$). In this chapter, to keep moderate the dimension of the parameterisation space, only filters with the same scale along the axes are considered.

Regarding the MLDF filters, they can be parameterised in terms of the number of positive/negative lobes, location, scale, orientation and inter-lobe distance. To keep the number of possibilities moderately low, only Gaussian kernels with balanced number of positive / negative lobes (1/1, 2/2, ...) and equal scale for both types of lobes are considered. Hence, the MLDF filters are expressed by:

$$\mathbf{m}[\mathbf{x_j},\mu_\mathbf{j},\sigma_\mathbf{j}] = \sum_{j=1}^{t_l}(-1)^{j+1}\frac{1}{\sqrt{2\pi\sigma_j}}\exp\left[\frac{-(\mathbf{x_j}-\mu_\mathbf{j})^\mathbf{2}}{2\sigma_j}\right], \tag{3}$$

where $\mathbf{x_j}=(x_j,y_j)$ is the centre of each of the $t_l$ lobes. Next, $\boldsymbol{k}=\{\boldsymbol{m},\boldsymbol{g}\}$ filters were convolved with each normalized iris image $\boldsymbol{I}$, providing a set of coefficients. The sign of the coefficients was obtained, i.e., $\boldsymbol{C}$ is the vector representation of $\text{sgn}(\boldsymbol{I}*\boldsymbol{k})$. In terms of parameterisations tested per filter, for Gabor kernels the wavelength (px.) $\omega : \{1:1:14\}$, the orientation $\varphi : \{0,\pi/4,\pi/2,3\pi/4\}$ and the Gaussian sigma $\sigma : 0.65\omega$. Regarding MLDFs, the number of lobes $t_l : \{1/1,2/2,3/3,4/4\}$ and the Gaussian sigma $\sigma : \{1,2,3,4,5,6\}$.

**Table 3** Types and range of the filters parameters varied in our experiments.

| **Gabor Filters** $\boldsymbol{g}[.,.]$ | |
|---|---|
| Wavelength (px.) | $\omega : \{1:1:14\}$ |
| Orientation | $\varphi : \{0,\pi/4,\pi/2,3\pi/4\}$ |
| Gaussian Sigma | $\sigma : 0.65\omega$ |
| **MLDF Filters** $\boldsymbol{m}[.,.]$ | |
| Num. Lobes | $t_l : \{1/1,2/2,3/3,4/4\}$ |
| Gaussian Sigma | $\sigma : \{1,2,3,4,5,6\}$ |

Fig. 7 illustrates the filters used and Table 3 summarizes the range of parameters considered, with ($\{a:b:c\}$ denoting values in the $[a,c]$ interval, with steps of size $b$).

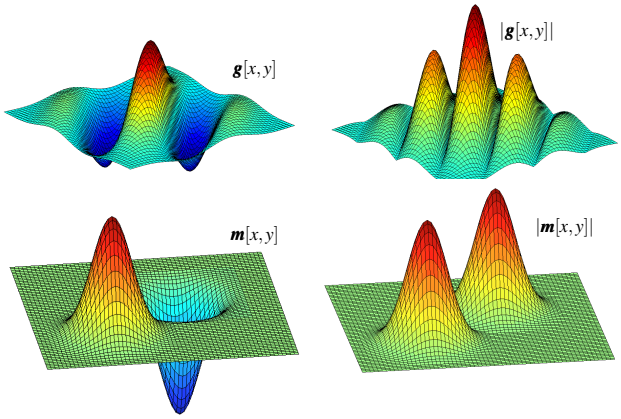


**Fig. 7** Illustration of the filters used in experiments ($\{g,m\}$) and of the filters that give the contribution of each position in the iris to the coefficient in the iris code $\{|g|,|m|\}$.

Fig. 8 expresses the variations in discriminability with respect to each parameter of the filters. The continuous lines represent the BATH dataset, the dashed lines with the diamond marks regard the CASIA-Iris-Distance. The UBIRIS.v2 is given by the dotted lines with triangular marks and the FRGC dataset by the dashed lines with circular marks. Above each plot we illustrate a normalized iris image and represent the filters that correspond to the nearby positions in the plot. Generally, the discriminability was substantially higher for MLDF than for Gabor filters. In case of the latter filters, larger wavelengths consistently increased the discriminability, essentially because they have a reduced sensitivity to outlier values due to acquisition artefacts. Orientation is another relevant parameter for Gabor kernels, where filters that analyze features that spread radially in the normalized data provided much better results. Regarding MLDF filters, filters with more lobes got worse results, which might be due to the *cross-elimination* effect of differences between lobes. Surprisingly, the variation in results with respect to the sigma of the Gaussian kernel are not so evident as in the case of Gabor kernels.

## *6.2 Analysis of Iris Codes: Comparison Between NIR and VW Data*

The discriminability $\tau$ of each bit extracted from NIR and VW images was obtained. Note that the iris patches evolved in the convolution for each bit contribute to the result in different degree, according to the magnitude of the kernel at each point, i.e., if a kernel has very small value at a specific position, the corresponding intensity

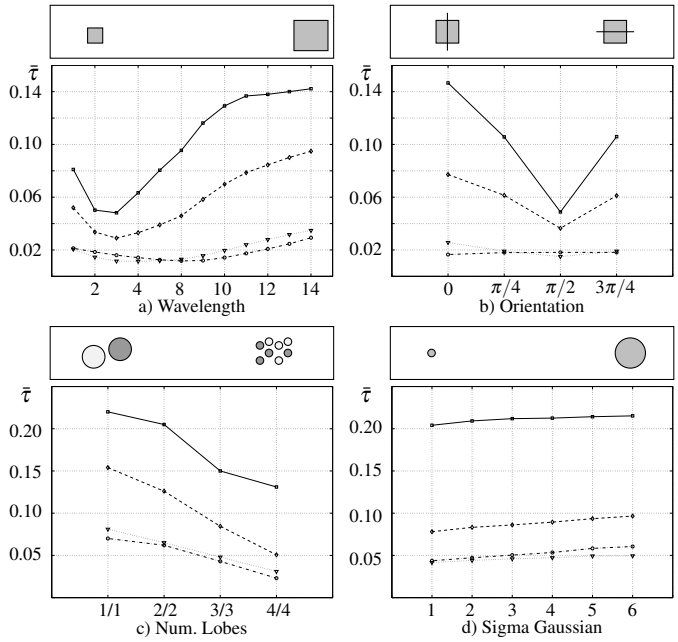


**Fig. 8** Average discriminability $\bar{\tau}$ of the bits in iris codes, regarding filters parameterization. The upper row regards the Gabor kernels (wavelength and orientation parameters) and the bottom row corresponds to the MLDF filters (number of lobes and sigma of the Gaussian kernel).

on the patch almost does not affect the result. This way, the contribution of each location $[x,y]$ in the iris to the bit value is given by:

$$\Psi[x,y] = \frac{\sum_i \left( |\boldsymbol{k_i}[x-r_i, y-c_i]|\ \tau(i) \right)}{\sum_i |\boldsymbol{k_i}[x-r_i, y-c_i]|}, \tag{4}$$

where $[r_i, c_i]$ is the central position of the i$^{th}$ filter $\boldsymbol{k_i}$ and $\tau(i)$ is the discriminability of the i$^{th}$ bit, given by:

$$\tau(i) = P(C_i^{(p)} \oplus C_i^{(q)} = 0\ |H_a) - P(C_i^{(p)} \oplus C_i^{(q)} = 0\ |H_0), \tag{5}$$

with $P(C_i^{(p)} \oplus C_i^{(q)} = 0\ |H_a)$ expressing the probability that the the i$^{th}$ bit of an iris code is equal in two inter-subject samples, and $P(C_i^{(p)} \oplus C_i^{(q)} = 0\ |H_0)$ expressing the same probability for intra-subject samples.

Fig. 9 gives the discriminability provided by each region of the iris in the Cartesian and polar coordinate systems, when using Gabor filters. Complementary, Fig. 10 expresses the similar statistics when using MLDF filters. The immediate

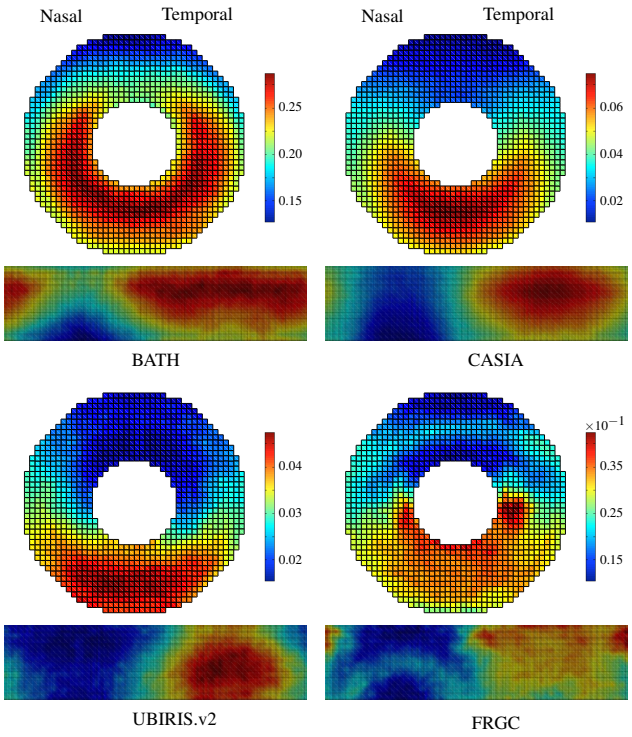


**Fig. 9** Average bit discriminability $\Psi[x,y]$ across the iris, using Gabor filters as feature encoders. Values are given for the Cartesian and polar coordinate systems, for the four data sets considered: BATH and CASIA-Iris-Distance (NIR) and UBIRIS.v2 and FRGC (VW).

conclusion is that the maximal values are observed for the NIR data sets, both for Gabor and MLDF filters. Interestingly, in all cases the lower parts of the iris are better than the upper parts, which are more frequently occluded by eyelids. Globally, MLDF filters provided more homogeneous values than Gabor filters. For VW data, regions nearby the pupillary boundary are worse than the middle and outer bands, probably due to the difficulty in obtaining reliable estimates of the pupillary boundary in VW images.

Regarding the radial bands in the iris, even though the maximal discriminability was observed for the middle bands, this might not be due to biological properties of the iris texture. Instead, the middle bands are the regions where the largest filters can be applied without surpassing the iris boundaries. As illustrated in Fig. 8, large filters tend to produce more discriminant bits, which accords with the results given in [27].

It is interesting to note the reduced correlation between the amounts of information in iris patches and the discriminability of each patch. For the BATH data set,

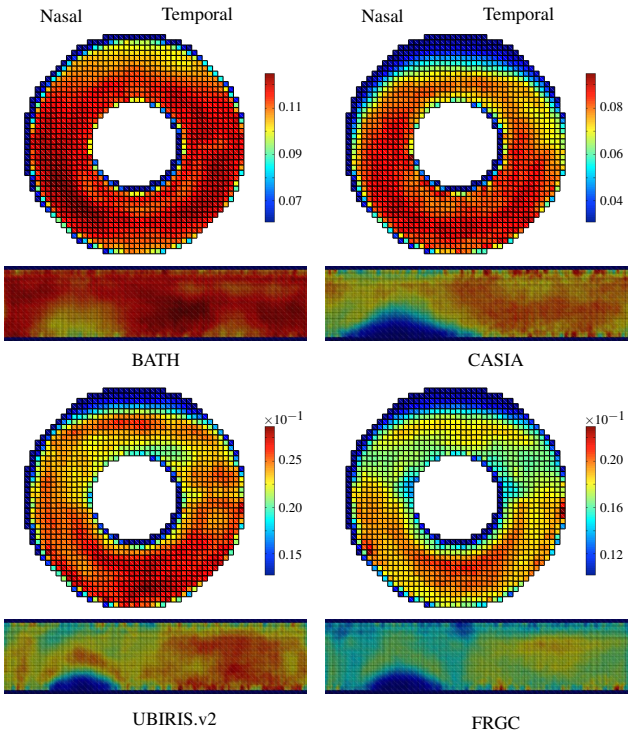


**Fig. 10** Average bit discriminability $\Psi[x,y]$ across the iris, using Multi-Lobe Differential Filters as feature encoders. Values are given for the Cartesian and polar coordinate systems, for the four data sets considered: BATH and CASIA-Iris-Distance (NIR) and UBIRIS.v2 and FRGC (VW).

the observed levels of linear correlation between variables $h[x,y]$ and $\Psi[x,y]$ are -0.12/-0.38 (Gabor/MLDF filters), and -0.40/-0.22 for the CASIA-Iris-Distance set. Regarding the VW data, values are 0.16/-0.02 for the UBIRIS.v2 and -0.34/-0.41 for the FRGC datasets. These low correlation values in terms of magnitude and sign (negative in 7/8 of the cases) give space for additional research about iris feature extraction / matching strategies that profit in a better way from the amount of information that is locally available.

In summary, MLDFs appear to provide better performance than Gabor kernels due to their ability of exploiting non-adjacent patterns. This property is particularly interesting for tissues with interlacing fibers, such as the human iris; 2) there is a strong agreement between the best iris regions obtained for MLDF and Gabor filters, suggesting that the choice for the best regions to perform iris recognition is relatively independent of the kind of filters used.

## *6.3 Codes Quantization: Is Too Much Information Lost?*

In the most acknowledged iris recognition algorithm, only phase information is used in recognition. Amplitude information is not considered reliable, as it depends of imaging contrast, illumination and camera gain. Accordingly, Hollingsworth *et* al. [27] observed that most inconsistencies in iris codes are due to the coarse quantization of the phase response, and disregarded bits from filter responses near the axes.

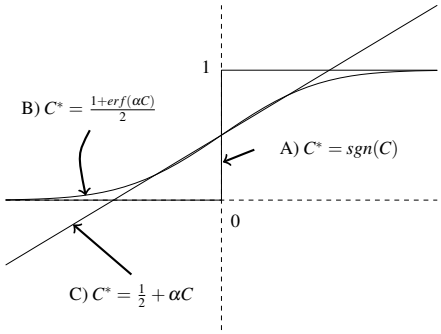


**Fig. 11** Three different strategies for code quantization: A) binary; B) sigmoid function; and C) linear mapping.

Even considering the above arguments reasonable, we assessed the amounts of discriminating information contained in the filter responses near the axes. With respect to the traditional strategy of keeping only the sign of coefficients (function A) in Fig. 11), two other strategies are considered: a linear mapping of the magnitude of the responses, yielding real-valued coefficients matched by the $\ell_2$ norm (function C) in Fig. 11); and a trade-off of both strategies, according to a sigmoid-based transform that maps large magnitude values to the 0/1values, but weights values near the axes to real values in the [0,1] interval. In this case, the $\ell_2$ norm was also used as matching function.

The ROC curves given at the right side of Fig. 12 compare the recognition performance with respect to each quantization strategy and Table 4 summarizes the results, giving the Area Under Curve (AUC) and the decidability index d' that, as suggested by Daugman [14], measures how well separated the genuine / impostor distributions are:

$$d' = \frac{|\mu_G - \mu_I|}{\sqrt{\frac{1}{2}(\sigma_I^2 + \sigma_G^2)}}, \tag{6}$$

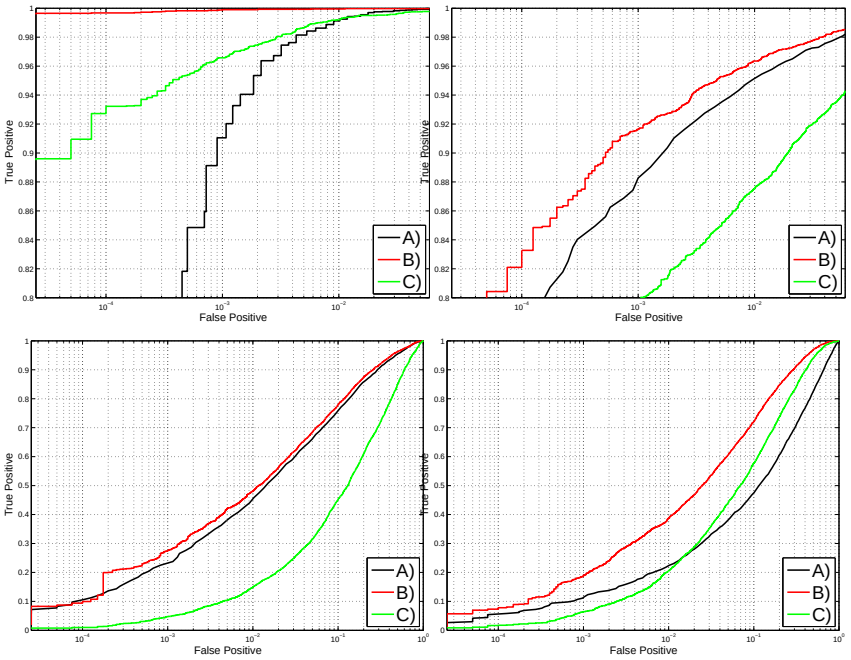


**Fig. 12** Rcognition performance with respect to A), B) and C) code quantization strategies for BATH (upper-left plot), CASIA-Iris-Distance (upper-right), UBIRIS.v2 (bottom-left) and FRGC data sets (bottom-right).

where $\mu_I = \frac{1}{k}\sum_i d_i^I$ and $\mu_G = \frac{1}{m}\sum_i d_i^G$ are the means of the genuine (G) and impostor (I) scores and $\sigma_I = \frac{1}{k-1}\sum_i (d_i^I - \mu_I)^2$ and $\sigma_G = \frac{1}{m-1}\sum_i (d_i^G - \mu_G)^2$ their standard deviations.

Two opposite conclusions can be drawn: for Gabor filters, the best results are observed when using the traditional sign() quantization function. In this case, using scalars instead of sign bits even decreased the recognition performance. Oppositely, for MLDF filters, the best results are observed when using the proposed sigmoid function, i.e., when the coefficients of small magnitude are also considered for the matching process. This points toward the conclusion that there is actually reliable discriminating information in the coefficients near the origin. However, these coefficients are less reliable than those with large magnitude, as in no case the linear mapping strategy got results close to any of the remaining strategies.

Note that the above conclusions result from the reported AUC and d' values, which in the large majority of the cases are in agreement. The exceptions occur mostly in cases where the shape of the genuine / impostor distributions are the farthest from Gaussian distributions. For these particular cases, we relied mostly on the AUC value, as it does not require a specific data distribution to report meaningful results.

**Table 4** Variations in recognition performance with respect to different strategies for code quantization.

| | | A) sign() | | B) sigmoid() | | C) linear (no quantization) | |
|---|---|---|---|---|---|---|---|
| **Dataset** | **Features** | **d'** | **AUC** | **d'** | **AUC** | **d'** | **AUC** |
| BATH | Gabor | $\mathbf{8.79 \pm 0.01}$ | $\mathbf{0.994 \pm 0.001}$ | $7.08 \pm 0.01$ | $0.992 \pm 0.001$ | $6.52 \pm 0.01$ | $0.990 \pm 0.001$ |
| BATH | MLDF | $\mathbf{9.15 \pm 0.01}$ | $\mathbf{0.994 \pm 0.001}$ | $8.82 \pm 0.01$ | $0.993 \pm 0.001$ | $5.89 \pm 0.01$ | $0.988 \pm 0.001$ |
| CASIA-Iris-Distance | Gabor | $\mathbf{3.20 \pm 0.01}$ | $\mathbf{0.982 \pm 0.001}$ | $3.16 \pm 0.01$ | $0.982 \pm 0.001$ | $3.05 \pm 0.02$ | $0.971 \pm 0.001$ |
| CASIA-Iris-Distance | MLDF | $3.89 \pm 0.01$ | $0.990 \pm 0.001$ | $\mathbf{4.12 \pm 0.01}$ | $\mathbf{0.984 \pm 0.001}$ | $3.13 \pm 0.01$ | $0.982 \pm 0.001$ |
| UBIRIS.v2 | Gabor | $\mathbf{1.23 \pm 0.01}$ | $\mathbf{0.813 \pm 0.006}$ | $1.16 \pm 0.02$ | $0.793 \pm 0.007$ | $0.82 \pm 0.02$ | $0.720 \pm 0.006$ |
| UBIRIS.v2 | MLDF | $1.88 \pm 0.01$ | $0.904 \pm 0.003$ | $\mathbf{1.96 \pm 0.01}$ | $\mathbf{0.917 \pm 0.003}$ | $1.02 \pm 0.01$ | $0.766 \pm 0.009$ |
| FRGC | Gabor | $\mathbf{1.12 \pm 0.02}$ | $\mathbf{0.792 \pm 0.006}$ | $1.01 \pm 0.02$ | $0.770 \pm 0.008$ | $0.83 \pm 0.01$ | $0.731 \pm 0.007$ |
| FRGC | MLDF | $1.74 \pm 0.01$ | $0.892 \pm 0.006$ | $\mathbf{1.88 \pm 0.02}$ | $\mathbf{0.908 \pm 0.002}$ | $1.47 \pm 0.02$ | $0.849 \pm 0.007$ |

# 7 Ocular Recognition

As an attempt to increase the robustness of iris recognition in visible-light data, the concept of *periocular* biometrics has emerged, which compensates for the degradation in iris data by considering the discriminating information in the surroundings of the eye (eyelids, eyelashes, eyebrows and skin texture). Currently, the most relevant algorithms work in a holistic way: they define a region-of-interest (ROI) around the eye and use a feature encoding / matching algorithm regardless of the biological component in each point of the ROI. However, this augments the probability of sensitivity to some data covariate and the correlation between the scores extracted from the different points in the ROI.

## *7.1 Weak / Strong Ocular Experts*

Under an atomistic criterion, two experts that use disjoint data can be devised, with radically different recognition strategies and attaining very different effectiveness. Here, the term *weak* is employed to refer to a recognition system that yields a poor separable decision environment, i.e., where the distributions of the genuine / impostor pairwise scores largely overlap. The term *strong* refers to a system where the distributions of genuine and impostor scores almost don't overlap, resulting in a clearly separable decision environment and low error rates.

In this dual ensemble, the strong expert analyses the multi-spectral information in the iris texture, according to an automatically optimised set of multi-lobe differential filters (MLDF). Complementary, the weak expert parameterises the boundary of the visible cornea and defines a dimensionless ROI that comprises the eyelids, eyelashes and the surrounding skin. This expert helps to discriminate between individuals and has three interesting properties: 1) it analyses data that has an appearance independent of the iris texture; 2) it shows reduced sensitivity to the most problematic iris image covariates; and 3) it exclusively analyses traits that cannot be easily forged by anyone not willing to be recognised, which is in contrast to the traits classically

used in periocular recognition (e.g., the shape of eyebrows). We encode the shape of eyelids, the distribution and shape of the eyelashes and the morphology of the skin wrinkles / furrows in the eyelids, which are determined by the movements of the *orbicularis oculi* muscles family. Fig. 13 overviews the information sources used in such recognition ensemble.

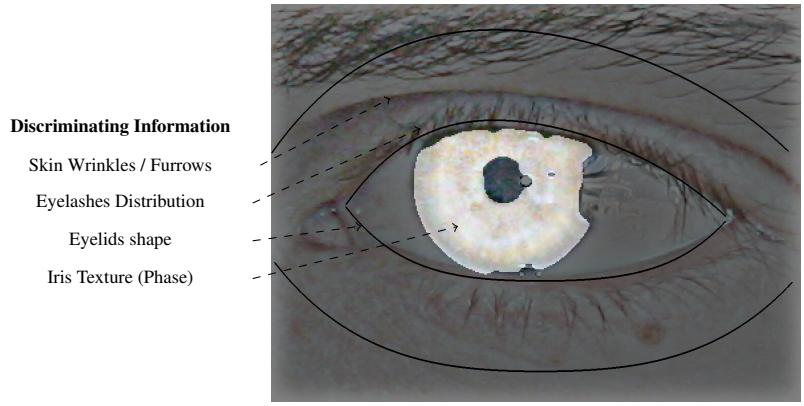


**Fig. 13** Overview of the components in the vicinity of the human eye that can be used to extract discriminating information, useful for biometric recognition purposes.

It is evident that using multiple sources for biometric recognition is not a new idea, and some controversy remains: is it actually an effective way to improve performance? It is argued that when a stronger and a weaker expert are combined, the resulting decision environment is averaged and the performance will be somewhere between that of the two experts considered individually [14]. Due to the way such a strong / weak ensemble was designed, our experiments support a radically different conclusion: even when the fused responses come from experts with very distant performance, the ensemble attains much better performance than the stronger expert (iris). This is due to the fact that both experts produce quasi-independent responses and are not particularly sensitive to the same image covariate, augmenting the robustness against degraded data.

## *7.2 Relevant Ocular Recognition Algorithms*

Concluded in 2011, the *NICE: Noisy Iris Challenge Evaluation* [64] promoted the research about iris / ocular recognition in visible-light data. It received over one hundred participations and the best performing teams described their approaches

in two special issues of the *Image and Vision Computing*[4] and *Pattern Recognition Letters*[5] journals. This event has documented the state-of-the-art recognition performance, having the best algorithm achieved d-prime values above 2.57, area under curve around 0.95 and equal error rates of 0.12. This method (due to Tan *et* al. [80]) is actually a *periocular* recognition algorithm: texton histograms and semantic rules encode information from the surroundings of the eye, while ordinal measures and color histograms analyse the iris. The second best approach was due to Wang *et* al. [85] and is quite more classical: it employs an AdaBoost feature selection scheme from a large set of quantized Gabor-based features, matched by the Hamming distance.

The most relevant recognition algorithms for VW images can be divided with respect to their data source: 1) the iris; or 2) the periocular region. Regarding the first family, Raffei *et* al. [67] preprocessed the iris to remove reflections and represented the normalised data at multiple scales, according to the Radon transform. The score from each scale was matched by the Hamming distance and fused by weighted nonlinear combination. Rahulkar and Holambe [68] derived a wavelet basis for compact representation of the iris texture (triplet half-band filters), with coefficients matched by the minimum Cambera distance. A post-classifier outputs a match when more than $k$ regions give a positive response. Roy *et* al. [69] used a feature selection technique from game theory, based on coefficients from the Daubechies wavelet decomposition. The Hausdorff distance yields the matching score between two feature sets. Kumar and Chan [43] approached the problem from the data representation perspective, having used a quaternionic sparse coding scheme solved by convex optimisation. Quaternion image patches were extracted from the RGB channels and the basis pursuit algorithm used to find the quaternion coefficients. In another work [42], the same authors were based in the sparse representation for classification algorithm, using the output of a local Radon transform as feature space.

The second family of algorithms considers other data beside the iris (sclera, eyebrows and skin texture), and its popularity has been increasing since the work of Park *et* al. [55]. Bharadwaj *et* al. [5] fused a global descriptor (GIST) based on five perceptual dimensions (image naturalness, openness, roughness, expansion and ruggedness) to circular local binary patterns. The Chi-squared distance matched both types of features and a fusion scheme (score level) yielded the final matching value.

Crihalmeanu and Ross [12] used the sclera patterns as biometric trait. The sclera was segmented according to the pixel-wise proportion between the NIR and green channel values. After enhancing the blood vessels by a line filter, SURF, minutiae and correlation-based schemes produced the matching scores that were fused subsequently. Similarly, Zhou *et* al. [94] enhanced the blood vessels in the sclera by Gabor kernels and encoded features by line descriptors. The accumulated registration distance between pairs of line segments yielded the matching score. Also, Oh and Toh [52] encoded the information in the sclera by local binary patterns (LBP) in

[4] http://www.sciencedirect.com/science/journal/02628856/28/2

[5] http://www.sciencedirect.com/science/journal/01678655/33/8

angular grids, concatenated in a single feature vector. Then, a normalised Hamming distance produced the matching score.

In terms of hybrid approaches, Oh *et* al. [53] combined the sclera to periocular features. Directional features from the former region were extracted by structured random projections, complemented by binary features from the sclera. Tan and Kumar [79] fused iris information (encoded by Log-Gabor filters) to an over-complete representation of the periocular region (LBP, GIST, Histogram of Oriented Gradients and Leung-Malik Filters). Both representations were matched independently and fused at the score level.

**Table 5** State-of-the-art algorithms for recognising degraded ocular data acquired in visible light environments.

| **Method** | **Traits** | **Feat. Encoding** | **Feat. Matching** | **Performance** |
|---|---|---|---|---|
| Bharadwaj *et* al. [5] | Periocular (Holistic) | GIST, CLBP | Chi-square distance | 73% rank-1 (UBIRIS.v2) |
| Crihalmeanu and Ross [12] | Sclera | SURF, Minutiae (vessel bifurcations) | Euclidean distance, data correlation | EER $<$ 1.8% (Own dataset) |
| Kumar and Chan [43] | Iris | Quaternion Sparse Orientation Code | Shift Alignment | 48% rank-1 (UBIRIS.v2) |
| Kumar *et* al. [42] | Iris | Radon local transform | Sparse Representation for Classification | 40% rank-1 (UBIRIS.v2), 33% rank-1 (FRGC) |
| Oh and Toh [52] | Sclera | LBP | Hamming distance | EER 0.47% (UBIRIS.v1) |
| Oh *et* al. [53] | Periocular (Holistic), Sclera | Multi resolution LBP (Sclera), Directional Projections (Periocular) | Hamming and Euclidean distance | EER 5% (UBIRIS.v2) |
| Proença [65] | Periocular (Piecewise) | MLDF (iris), shape and texture descriptors (eyelashes, eyelids) | Modified Hamming (iris), Histogram distance (eyelids, eyelashes) | EER 2.97% (UBIRIS.v2) |
| Raffei *et* al. [67] | Iris | Multi-scale local Radon transform | Hamming distance, weighted non-linear score combination | AUC 88% (UBIRIS.v2) |
| Rahulkar and Holambe [68] | Iris | Triplet half-band filter bank | Canbera distance, k-out-of-n post classifier | Acc $>$ 99% (UBIRIS.v1) |
| Roy *et* al. [69] | Iris | Daubechies wavelet, Modified Contribution feature selection | Hausdorff distance | TPR 97.43%@ 0.001%FPR (UBIRIS.v1) |
| Tan and Kumar [79] | Iris, Periocular (Holistic) | Log-Gabor filters (Iris), SIFT, GIST, LBP, HOG and LMF (Periocular) | Chi-square and Euclidean distances | 39.4% rank-1 (UBIRIS.v2) |
| Tan *et* al. [80] | Iris, Eye | Texton Histograms, Semantic information (Eye), Ordinal Filters, Color Histogram (Iris) | Chi-square, Euclidean, Difusion and Hamming distances | AUC 95%(UBIRIS.v2) |
| Wang *et* al. [85] | Iris | Gabor filters, AdaBoost feature selection | Hamming distance | AUC 88% (UBIRIS.v2) |
| Zhou *et* al. [94] | Sclera | Line (sclera vessels) description | Accumulated line registration cost | EER 3.83% (UBIRIS.v2) |

Table 5 overviews the state-of-the-art algorithms in terms of biometric recognition from VW ocular data. It compares the analysed traits and summarises the techniques used in feature encoding and matching. The error rates reported by authors are also given (*Performance* column). However, note the above listed algorithms might have used different experimental protocols and data subsets, which turns the direct comparison of the error rates unfair.

Proença recently proposed a recognition ensemble [65] composed by two experts. The strong expert analyses the multi-spectral information in the iris texture, according to an automatically optimised set of multi-lobe differential filters (MLDF). Complementary, the weak expert parameterises the boundary of the visible cornea and defines a dimensionless ROI that comprises the eyelids, eyelashes and the surrounding skin. This expert helps to discriminate between individuals and has three interesting properties: 1) it analyses data that has an appearance independent of the iris texture; 2) it shows reduced sensitivity to the most problematic iris image covariates; and 3) it exclusively analyses traits that cannot be easily forged by anyone not willing to be recognised, which is in contrast to the traits classically used in periocular recognition (e.g., the shape of eyebrows).

The weak expert encodes the shape of eyelids, the distribution and shape of the eyelashes and the morphology of the skin wrinkles / furrows in the eyelids, which are determined by the movements of the *orbicularis oculi* muscles family. With respect to related works, the main advantage of this method is that the responses of the iris (strong) and ocular (weak) experts are practically independent, in result of the disjoint regions analyzed and in the fully disparate algorithms used in feature encoding / matching. This way, even by using relatively simple fusion techniques that work at the score level, it is possible to use the weak biometric expert as a valuable complement of the iris expert, particularly in cases where this expert produces matching scores that are near the borderline accept / reject regions. This kind of complementarity between experts is illustrated in Fig. 14, showing pairwise comparisons that are intra-subject (upper row) and inter-subject (bottom row), with $P_s$, $P_w$ denoting the posterior probability of acceptance (by the strong $s$ and weak $w$ experts) of the *null hypothesis* $H_0$ that both images are from the same subject.

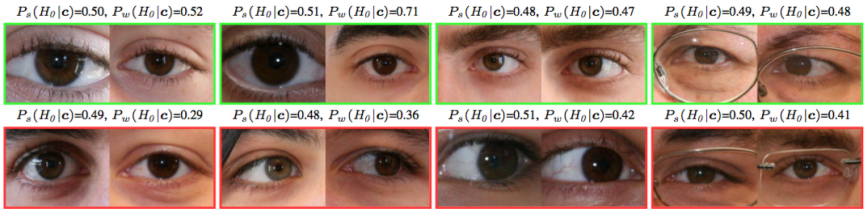


**Fig. 14** Examples of image pairwise comparisons that fall in the uncertainty region of the strong (iris) biometric expert ($P_s(H_0|x) \approx 0.5$) . In most cases, the weak (periocular) biometric expert provides valuable information $P_w$ to distinguish between intra-subject (green frames) and inter-subject comparisons (red frames).

## 8 Fusion of Multiple Recognition Systems

Considering that the type of biometric recognition systems discussed in this chapter should work covertly, meaning that no conscious human effort will be required of subjects during the recognition processes, there is a theoretically interesting possibility of using multiple recognition systems regularly spaced across an airport terminal hallway or a city street. This section reports the (optimistic) performance that such a recognition ensemble would attain, considering as baseline recognizers the current state-of-the-art solutions for *non-cooperative ocular recognition*.

It is known that not all subjects perform consistently in terms of false matches and non-matches of a biometric system. Based on their intrinsic features, some are difficult to match (*goats*), while others are particularly vulnerable to impersonation (*lambs*) and consistently increase the probability of false matches [88]. We oversimplify the problem and regard all subjects of a population $\mathbb{P} = \{s_1, \ldots, s_n\}$ as *sheep*, i.e., subjects that tend to follow the system averages: they match relatively well against themselves and poorly against others. Let us consider $k$ ocular recognition systems with roughly similar performance, with a sensitivity of $\alpha$ at a false match rate of $\beta$. Here we introduce the concept of *exogenous independence*, hypothesizing that purposely changing the lighting conditions in the environment (by using different levels of light or types of illuminants) and the acquisition protocols (poses, distances) should potentiate the independence between the system outputs. Assuming that the independence of each system provides an upper bound on the performance that would be attainable by the fusion of multiple systems, the binomial distribution can be used to obtain the probability that a subject $s_i$ is screened by $k$ recognition systems and correctly recognized by $k'$ of these, $1 \leq k' \leq k$:

$$P(R_{k'}) = \frac{k!}{k'!\,(k-k')!}\ \alpha^{k'}\ (1-\alpha)^{k-k'}. \tag{7}$$

For different values of $k'$, the probability that a reported match is false is given by $\beta^{k'}$, assuming that false matches in each of the $k$ recognition systems are independent events. Accordingly, a *match* will be reported *iff* a minimum of $k'$ recognition systems output a match:

$$\begin{aligned} P(R_{\geq k'}) &= \sum_{j=k'}^{k} P(R_j) \\ &= \sum_{j=k'}^{k} \frac{k!}{j!\,(k-j)!}\ \alpha^{j}\ (1-\alpha)^{k-j}, \end{aligned} \tag{8}$$

provided that all events are mutually exclusive. Considering the average performance for a baseline recognizer that fuses at the score level the responses given by four state-of-the-art algorithms ([80],[85], [71] and [73]), Fig. 15 gives the expected sensitivity of a *multipoint* biometric system, with respect to the number of baseline recognizers used, considering different false match rates. However, note

that this analysis provides an upper bound estimate of the ensemble performance, as it assumes that the responses given by individual experts are independent, Even though, this *optimistic* assumption would enable to conclude that around five independent recognition systems would be enough to attain almost full sensitivity at a false acceptance rate $\beta$ of 0.01. This value substantially increases when a lower number of false alarms is convenient (large scale applications), requiring between thirteen and twenty three independent recognition systems to operate, respectively, at FAR $1e^{-4}$ and $1e^{-6}$.

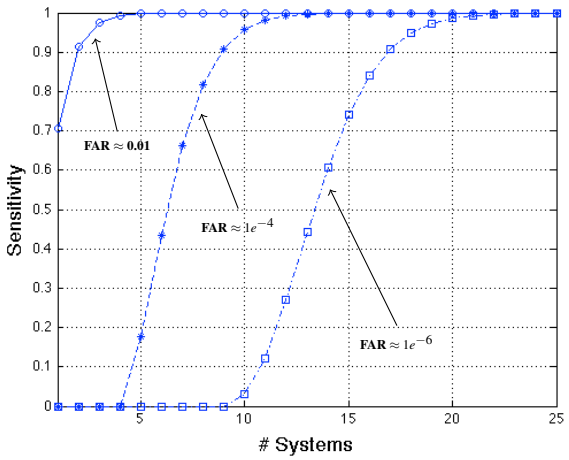


**Fig. 15** Expected sensitivity of an ensemble of ocular recognition systems working covertly and consecutively (e.g., in an airport terminal hallway or a city street), with different required values for the false acceptance rates. Note that this is an *optimistic* estimate of the ensemble performance, as it assumes that the responses given by baseline recognizers are statistically independent.

## 9 Conclusions and Current Challenges

There is no doubt that concerns about the security and safety of crowded urban areas have been increasing significantly, particularly due to terrorist attacks such as the 2001 New York 9/11, the 2004 Madrid train bombing and the 2013 Boston marathon attacks. These concerns raised the interests on biometrics and made it one the most popular topics in the Pattern Recognition / Computer Vision domains. However, there are still not biometric recognition systems that work effectively using data acquired in totally uncontrolled environments and without assuming subjects' willingness to be recognized.

This chapter discussed such extremely ambitious kind of biometric recognition and advocated the use of the ocular region as basis trait, due to several reasons: being a naturally protected internal organ visible from the exterior, it has a near circular and planar shape that turns easier its segmentation and parameterization. Also, its texture has a predominantly phenotypic or chaotic appearance that is stable over lifetime, which - particularly important - discriminating information between subjects lies in the lowest and middle-low frequency components, i.e., those that are easier to capture in unconstrained data acquisition protocols. Finally, the ocular region is less sensitive to facial expressions (than the whole face), and has a relatively small probability of being occluded due to hair, facial hair and clothing.

We started by summarising the most relevant research works devoted to increasing the recognition robustness with respect to data of reduced quality, and hereinafter, focused particularly in the major issues behind each of the phases that compose the recognition chain: data acquisition, segmentation, feature encoding and matching. Also, we summarized some of the most relevant works in the *periocular recognition* domain. In this topic, we stressed two key properties of an ocular recognition ensemble: 1) the *weak* (periocular) recognizer should provide as much independent scores (responses) as possible with respect to the *strong* (iris) recognizer; and 2) experts should not share particular sensitivity to the same data covariates, in order to actually improve recognition robustness.

Finally, the obstacles remaining in every phase of a fully *non-cooperative ocular recognition* system were discussed, particularly the difficulty in real-time detecting and segmenting all the components in the ocular region, which is important not only for developing non-holistic feature encoding / matching strategies, but also to estimate pose and data quality.

**Acknowledgements** The financial support given by "IT: Instituto de Telecomunicações" in the scope of the UID/EEA/50008/2013 project is acknowledged.

## References

1. Abhyankar A., Schuckers S.: Iris quality assessment and bi-orthogonal wavelet base decoding for recognition. *Pattern Recognition*, **42**, 1878–1894 (2009)
2. American National Standards Institute. American national standard for the safe use of lasers and LEDs used in optical fiber transmission systems, ANSI Z136.2 (1988)
3. Arvacheh E., Tizhoosh H.: A study on Segmentation and Normalization for Iris Recognition. M.Sc. dissertation, University of Waterloo (2006)
4. Basit A., Javed M.: Iris localization via intensity gradient and recognition through bit planes. In Proceedings of the *International Conference on Machine Vision*, 23–28 (2007)
5. Bharadwa S., Bhatt H., Vatsa M., Singh R.: Periocular biometrics: When iris recognition fails. In Proceedings of the *International Conference on Biometrics: Theory, Applications and Systems*, 1–6, U.S.A. (2010)
6. Boyce C., Ross A., Monaco M., Hornak L., Li X.: Multispectral iris analysis: A preliminary study. In Proceedings of the *First IEEE International Conference on Biometrics: Theory, Applications, and Systems*. 1–8, U.S.A. (2008)

7. Bowyer K., Hollingsworth K., Flynn P.: Image understanding for iris biometrics: A survey. Computer Vision and Image Understanding. **110**, 2 , 281–307 (2008)
8. Boddeti N., Kumar V.: Extended depth of field iris recognition with correlation filters. In Proceedings of the *Computer Vision and Pattern Recognition Workshop on Biometrics*, 51–59, U.S.A. (2006)
9. Broussard R., Kennell L., Soldan D., Ives R.: Using artificial neural networks and feature saliency techniques for improved iris segmentation. In Proceedings of the *International Joint Conference on Neural Networks*, 1283–1288 (2007)
10. Commission International de l'Eclarirage. Photobiological safety standards for safety standards for lamps. Report of TC 6-38, CIE 134-3-99 (1999)
11. Chen Y., Dass S., Jain A.: Localized iris image quality using 2-D wavelets. In Proceedings of the *International Conference on Biometrics*, 373–381 (2006)
12. Crihalmeanu S., Ross A.: Multispectral scleral patterns for ocular biometric recognition. *Pattern Recognition Letters*, **33**,14, 1860–1869 (2012)
13. Daugman J.: Uncertainty relation for resolution in space, spatial frequency, and orientation optimized by two-dimensional visual cortical filters. *Journal of the Optical Society of America - A*, **2**, 7, 1160–1169 (1985)
14. Daugman J.: Biometric decision landscapes. *University of Cambridge Technical Report*, UCAM-CL-TR-482, ISSN: 1476-2986 (2000)
15. Daugman J.: Probing the uniqueness and randomness of IrisCodes: Results from 200 billion iris pair comparisons. *Proceedings of the IEEE*, **94**(11), 1927–1935 (2006)
16. Daugman J.: New methods in iris recognition. *IEEE Transactions on Systems, Man, and Cybernetics - Part B: Cybernetics*, **37**(5) 1167–1175 (2007)
17. Daugman J., Downing C.: Effect of Severe Image Compression on Iris Recognition Performance. *IEEE Transactions on Information Forensic and Security*, **3**(1), 52–61 (2008)
18. Dobes M., Martineka J., Dobes D., Pospisil J.: Human eye localization using the modified hough transform. *Optik*, **117**, 468–473 (2006)
19. Du Y., Belcher C., Zhou Z.: Scale Invariant Gabor Descriptor-Based Noncooperative Iris Recognition. *EURASIP Journal on Advances in Signal Processing*, **2010**, ID 936512 (2010)
20. Fancourt C., Bogoni L., Hanna K., Guo Y., Wildes R., Takahashi N., Jain U.: Iris recognition at a distance. In Proceedings of the *2005 IAPR Conference on Audio and Video Based Biometric Person Authentication*, 1–13, U.S.A (2005)
21. Grabowski K., Sankowski W., Zubert M., Napieralska N.: Focus Assessment Issues in Iris Image Acquisition System. In Proceedings of the $14^{th}$ *International Conference MIXDES 2007*, 628–631 (2007)
22. He X., Shi P.: A new segmentation approach for iris recognition based on hand-heldcapture device. *Pattern Recognition*, **40**, 1326–1333 (2007)
23. He Y., Cui J.,Tan T., Wang Y.: Key techniques and methods for imaging iris in focus. In Proceedings of the *IEEE International Conference on Pattern Recognition*, 557–561, Hong Kong (2006)
24. He Z., Tan T., Sun Z.: Iris localization via pulling and pushing. In Proceedings of the $18^{th}$ *International Conference on Pattern Recognition*, **4**, 366–369 (2006)
25. He Z., Tan T., Sun Z., Qiu X.: Robust eyelid, eyelash and shadow localization for iris recognition. In Proceedings of the *International Conference on Image Processing*, 265–268 (2009)
26. Hollingsworth K., Bowyer K., Flynn P.: The Importance of small pupils: a study of how pupil dilation affects iris biometrics. In Proceedings of the *International Conference on Biometrics*, 1–6 (2008)
27. Hollingsworth K., Bowyer K., Flynn P.: The best bits in an iris code. *IEEE Transactions on Pattern Analysis and Machine Intelligence*, **31**(6), 964–973 (2009)
28. Honeywell International Inc.: A distance iris recognition. United States Patent 20070036397 (2007)
29. Honeywell International Inc. : Invariant radial iris segmentation, United States Patent 20070211924 (2007)
30. International Biometric Group: Independent test of iris recognition technology, `http://www.biometricgroup.com/reports` (2005)

31. Jang J., Park K., Kim J., Lee Y.: New focus assessment method for iris recognition systems. *Pattern Recognition Letters*, **29**(13), 1759–1767 (2008)
32. Li P., Ma H.: Iris Recognition in Non-ideal Imaging Conditions. *Pattern Recognition Letters*, **33**(8), 1012–1018 (2012)
33. Li P., Liu X., Zhao N.: Weighted Co-occurrence Phase Histogram for Iris Recognition. *Pattern Recognition Letters*, **33**(8), 1000-1005 (2012)
34. Lu G, Qi J., Liao Q.: A New Scheme of Iris Image Quality Assessment. InProceedings of the *Third International Conference on International Information Hiding and Multimedia Signal Processing*, **1**, 147–150 (2007)
35. Marsico M., Nappi M., Riccio D.: Noisy Iris Recognition Integrated Scheme. *Pattern Recognition Letters*, **33**(8), 1006–1011 (2012)
36. Kalka N., Zuo J., Schmid N., Cukic B.: Estimating and Fusing Quality Factors for Iris Biometric. *IEEE Transactions on Systems, Man and Cybernetics, Part A*, **40**(3), 509–524 (2010)
37. Kang B., Park K.: A study on iris image restoration. In Proceedings of the *International Conference on Audio- and Video-Based Biometric Person Authentication*, 31–40 (2005)
38. Kang B., Park K.: A Robust eyelash detection based on iris focus assessment. *Pattern Recognition Letters*, **28**(13), 1630–1639 (2007)
39. Kang B., Park K.: A new multi-unit iris authentication based on quality assessment and score level fusion for mobile phones. *Machine Vision and Applications, DOI: 10.1007/s00138-009-0184-0* (2009)
40. Kennell L., Ives R., Gaunt R.: Binary morphology and local statistics applied to iris segmentation for recognition. In Proceedings of the *IEEE International Conference on Image Processing*, 293–296 (2006)
41. Krichen E. Garcia-Salicetti S., Dorizzi B.: A new probabilistic iris quality measure for comprehensive noise detection. In Proceedings of the *International Conference on Biometrics: Theory, Applications, and Systems*, 1–6 (2007)
42. Kumar A., Chan T-S., Tan C-W.: Human identification from at-a-distance face images using sparse representation of local iris features. In Proceedings of the *International Conference on Biometrics*, 303–309 (2012)
43. Kumar A., Chan T-S.: Iris recognition using quaternionic sparse orientation code (QSOC). In Proceedings of the *Computer Vision and Pattern Recognition Workshops*, 59–64 (2012)
44. Liu X., Bowyer K., Flynn P.: Experiments with an improved iris segmentation algorithm. In Proceedings of the *Fourth IEEE Workshop on Automatic Identification Advanced Technologies*, 118–123 (2005)
45. Maddalena L., Petrosino A.: The SOBS algorithm: What are the limits? In Proceedings of the *Computer Vision and Pattern Recognition Workshops*, 21–26 (2012)
46. Matey J. R., Ackerman D., Bergen J., Tinker M.: Iris recognition in less constrained environments. *Springer Advances in Biometrics: Sensors, Algorithms and Systems*, 107–131 (2007)
47. Mansfield T.,Kelly G., Chandler D., Kane J.: Biometric product testing final report. issue 1.0 (2001)
48. Meredith P, Sarna T.: The physical and chemical properties of eumelanin. Pigment Cell Research, **19**, 572–594 (2006)
49. Morimoto C., Santos T., Muniz A.: Automatic iris segmentation using active near infra red lighting. In Proceedings of the *Brazilian Symposium on Computer Graphics and Image Processing (SIBGRAPI 2005)*, 37–43 (2005)
50. Nandakumar K., Chen Y., Jain A., Dass S.: Quality based score level fusion in multibiometric systems. In Proceedings of the*International Conference on Pattern Recognition*, 473–476 (2006)
51. Narayanswamy R., Johnson G., Silveira P., Wach H.: Extending the imaging volume for biometric iris recognition. *Applied Optics*, **44**(5), 701–712 (2005)
52. Oh K., Toh K-A.: Extracting sclera features for cancellable identity verification. in Proceedings of the *International Conference on Biometrics*, 245–250 (2012)
53. Oh K., Oh B-S., Toh K-A., Yau W-Y., Eng H-L.: Combining sclera and periocular features for multi-modal identity verification. *Neurocomputing*, DOI: `10.1016/j.neucom.2013.01.066` (2013)

54. Park K., Kim J.: A real-time focusing algorithm for iris recognition camera. *IEEE Transactions on Systems, Man and Cybernetics*, **35**(3), 441–444 (2005)
55. Park U., Jilela R., Ross A., Jain A.K.: Periocular Biometrics in the Visible Spectrum. *IEEE Transactions on Information Forensics and Security*, **6**(1), 96–106 (2011)
56. Phillips P., Flynn P., Scruggs T., Bowyer K., Chang J., Hoffman K.: Overview of the face recognition grand challenge. In Proceedings of the *IEEE Conference on Computer Vision and Pattern Recognition*,1, 947–954 (2005)
57. Poursaberi A, Araabi B.: Iris recognition for partially occluded images methodology and sensitivity analysis. *EURASIP Journal on Advances in Signal Processing*, **2007**, 20–32 (2007)
58. Proença H., Alexandre L.: Iris segmentation methodology for non-cooperative iris recognition. *IEE Proc. Vision, Image & Signal Processing*, **153**(2), 199–205 (2006)
59. Proença H., Alexandre L.: A method for the identification of noisy regions in normalized iris images. In Proceedings of the *International Conference on Pattern Recognition*, **4**, 405–408 (2006)
60. Proença H., Filipe S., Santos R., Oliveira J., Alexandre L.: The UBIRIS.v2: A Database of Visible Wavelength Iris Images Captured On-The-Move and At-A-Distance. *IEEE Transactions on Pattern Analysis and Machine Intelligence*, **32**(8), 1529–1535 (2010)
61. Proença H.: Iris Recognition: On the Segmentation of Degraded Images Acquired in the Visible Wavelength. *IEEE Transactions on Pattern Analysis and Machine Intelligence*, **32**(8), 1502–1516 (2010)
62. Proença H., Alexandre L.: Iris recognition: Analysis of the error rates regarding the accuracy of the segmentation stage. *Image and Vision Computing*, **28**, 202–206 (2010)
63. Proença H.: Quality Assessment of Degraded Iris Images Acquired in the Visible Wavelength. *IEEE Transactions on Information Forensics and Security*, **6**(1), 82–95 (2011)
64. Proença H., Alexandre L.: Toward Covert Iris Biometric Recognition: Experimental Results From the NICE Contests. *IEEE Transactions on Information Forensics and Security*, **7**(2), 798–808 (2012)
65. Proença H.: Ocular Biometrics by Score-Level Fusion of Disparate Experts. *IEEE Transactions on Image Processing*, **31**(12), 5082–5093 (2014)
66. Puhan N., Jiang X.: Robust eyeball segmentation in noisy iris images using fourier spectral density. In Proceeding of the $6^{th}$ *IEEE International Conference on Information, Communications and Signal Processing*, 1–5 (2007)
67. Raffei A., Asmundi H., Hassan R., Othman R.: Feature extraction for different distances of visible reflection iris using multiscale sparse representation of local Radon transform. *Pattern Recognition*, **46**, 2622–2633 (2013)
68. Rahulkar A.,Holambe R.: Half-Iris Feature Extraction and Recognition Using a New Class of Biorthogonal Triplet Half-Band Filter Bank and Flexible k-out-of-n:A Postclassifier. *IEEE Transactions on Information Forensics and Security*, **7**(1), 230–240 (2012)
69. Roy K., Battacharya P., Suen C.: Iris recognition using shape-guided approach and game theory. *Pattern Analysis and Applications*, **14**, 329–348 (2011)
70. Ross A., Shah S.: Segmenting non-ideal irises using geodesic active contours. In Proceedings of the *IEEE 2006 Biometric Symposium*, 1–6 (2006)
71. Santos G., Hoyle E.: A Fusion Approach to Unconstrained Iris Recognition. *Pattern Recognition Letters*, **33**(8), 984–990 (2012)
72. Shi, J., Tomasi, C.: Good features to track.. In Proceedings of the *IEEE Computer Society Conference on Computer Vision and Pattern Recognition*. U.S.A (1994)
73. Shin K., Nam G., Jeong D., Cho D., Kang B., Park K., Kim J.: New Iris Recognition Method for Noisy Iris Images. *Pattern Recognition Letters*, **33**(8), 991–999 (2012)
74. Schuckers S., Schmid N., Abhyankar A., Dorairaj V., Boyce C., Hornak L.: On techniques for angle compensation in nonideal iris recognition. *IEEE Transactions on Systems, Man and Cybernetics-Part B: Cybernetics*, **37**(5), 1176–1190, (2007)
75. Smith K., Pauca V., Ross A., Torgersen T., King M.: Extended evaluation of simulated wavefront coding technology in iris recognition. In *Proceedings of the First IEEE International Conference on Biometrics: Theory, Applications, and Systems*. 1–7, U.S.A (2007)

76. Sun Z., Tan T.: Ordinal Measures for Iris Recognition. *IEEE Transactions on Pattern Analysis and Machine Intelligence*, **23**(12), 2211–2226 (2009)
77. Szewczyk R., Grabowski K., Napieralska M., Sankowski W., Zubert M., Napieralski A.: Reliable Iris Recognition Algorithm Based on Reverse Biorthogonal Wavelet Transform. *Pattern Recognition Letters*, **33**(8), 1019-1026 (2012)
78. Tan T., He Z., Sun Z.: Efficient and robust segmentation of noisy iris images for non-cooperative segmentation. *Image and Vision Computing*, **28**(2), 223-230 (2010)
79. Tan C-W., Kumar A.: Towards Online Iris and Periocular Recognition Under Relaxed Imaging Constraints. *IEEE Transactions on Image Processing*, **22**(10), 3751–3765 (2013)
80. Tan T., Zhang X., Sun Z., Zhang H.: Noisy iris image matching by using multiple cues. *Pattern Recognition Letters*, **33**(8), 970–977 (2012)
81. Turk M., Pentland A.: Eigenfaces for Recognition. *Journal of Cognitive Neuroscience*, **3**(1), 71–86 (1991)
82. Vatsa M, Singh R., Noore A.: Improving iris recognition performance using segmentation, quality enhancement, match score fusion, and indexing. *IEEE Transactions on Systems, Mans and Cybernetics - B*, **38**(4), 1021–1035 (2008)
83. Viola, P., Jones, M.: Rapid object detection using a boosted cascade of simple features. In Proceedings of the *2001 IEEE Computer Society Conference on Computer Vision and Pattern Recognition*, **1** (2001)
84. Wan J., He X., Shi P.: An Iris Image Quality Assessment Method Based on Laplacian of Gaussian Operation. In Proceedings of the *IAPR Conference on Machine Vision Applications*, 248–251 (2007)
85. Wang Q., Zhang X., Li M., Dong X., Zhou Q. Yin Y.: Adaboost and multi-orientation 2D Gabor-based noisy iris recognition. *Pattern Recognition Letters*, **33**, 978–983 (2012)
86. Wei Z., Tan T, Sun Z., Cui J.: Robust and Fast Assessment of Iris Image Quality. In Proceedings of the *International Conference on Biometrics*, 464–471 (2006)
87. Xu Z., Shi P.: A robust and accurate method for pupil features extraction. In Proceedings of the $18^{th}$ *International Conference on Pattern Recognition*, **1**, 437–440 (2006)
88. Yager N., Dunstone T.: The Biometric Menagerie.. *IEEE Transactions on Pattern Analysis and Machine Intelligence*, **32**(2), 220–230 (2010)
89. Ye X., Yao P., Long F., Zhuang Z.: Iris image realtime pre-estimation using compound neural network. In Proceedings of the *International Conference on Biometrics*, 450–456 (2006)
90. Yoon S., Bae K.,Ryoung K., Kim P.: Pan-tilt-zoom based iris image capturing system for unconstrained user environments at a distance. *Lecture Notes in Computer Science*, **4642**, 653–662, U.S.A (2007)
91. Zaim A.: Automatic segmentation of iris images for the purpose of identification. In Proceedings of the *IEEE International Conference on Image Processing*, **3**, 11–14 (2005)
92. Zhang G., Salganicoff M.: Method of measuring the focus of close-up image of eyes. U.S. Patent No. 5,953,440 (1999)
93. Zheng Z., Yang J., Yang L.: A robust method for eye features extraction on color image. *Pattern Recognition Letters*, **26**, 2252–2261 (2005)
94. Zhou Z., Du E., Thomas N., Delp E.: A New Human Identification Method: Sclera Recognition. *IEEE Transactions on Systems, Man and Cybernetics - Part A: Systems and Humans*, **42**(3), 571–583 (2012)
95. Zuo J., Kalka N., Schmid N.: A robust iris segmentation procedure for unconstrained subject presentation. In Proceedings of the *Biometric Consortium Conference*, 1–6 (2006)
96. Zuo J., Schmid N.: An automatic algorithm for evaluating the precision of iris segmentation. In Proceedings of the *IEEE Conference on Biometrics: Theory, Applications and Systems*, 1–6 (2008)
97. Zuo J., Schmid N.: Global and local quality measures for NIR iris video. In Proceedings of the *International Conference On Computer Vision and Pattern Recognition*, 120–125 (2009)